


Propagation and synchronization of reverberatory bursts in developing cultured networks

Chih-Hsu Huang¹ · Yu-Ting Huang^{1,2} · Chun-Chung Chen¹  · C. K. Chan^{1,2}

Received: 20 May 2016 / Revised: 14 November 2016 / Accepted: 21 November 2016 / Published online: 9 December 2016
© Springer Science+Business Media New York 2016

Abstract Developing networks of neural systems can exhibit spontaneous, synchronous activities called neural bursts, which can be important in the organization of functional neural circuits. Before the network matures, the activity level of a burst can reverberate in repeated rise-and-falls in periods of hundreds of milliseconds following an initial wave-like propagation of spiking activity, while the burst itself lasts for seconds. To investigate the spatiotemporal structure of the reverberatory bursts, we culture dissociated, rat cortical neurons on a high-density multi-electrode array to record the dynamics of neural activity over the growth and maturation of the network. We find the synchrony of the spiking significantly reduced following the initial wave and the activities become broadly distributed spatially. The synchrony recovers as the system reverberates until the end of the burst. Using a propagation model we infer the spreading speed of the spiking activity, which increases as the culture ages. We perform computer simulations of the system using a physiological model of spiking networks in two

spatial dimensions and find the parameters that reproduce the observed resynchronization of spiking in the bursts. An analysis of the simulated dynamics suggests that the depletion of synaptic resources causes the resynchronization. The spatial propagation dynamics of the simulations match well with observations over the course of a burst and point to an interplay of the synaptic efficacy and the noisy neural self-activation in producing the morphology of the bursts.

Keywords Bursting · Reverberation · Synchronization · Cultured network · Simulation

1 Introduction

During the development of neural systems, spontaneous and synchronous activities can appear following the outgrowth of neurites and before the availability of external stimulus inputs (Segev et al. 2003; Meister et al. 1991). These activities are believed to play an important role in the formation and organization of functional neural circuitries (Katz and Shatz 1996; Turrigiano and Nelson 2004; Harris 1981; Crair 1999). The investigation of these network activities can help to elucidate the cellular and network mechanisms involved in neural development (Zhang and Poo 2001; Bi and Poo 2001; Blankenship and Feller 2010; Kerschensteiner 2014) and will lead to a better understanding of the functioning of a brain (Penn and Shatz 1999; Hua and Smith 2004; Chippalone et al. 2006; Pu et al. 2013). Among approaches to study the spontaneous activity of developing neural systems, dissociated cultures of cortical or hippocampal neurons on a multi-electrode array (MEA) have been used for decades as experimental models for observing the dynamics of growing networks (Thomas et al. 1972; Pine 1980; Gross et al. 1982; Potter and DeMarse 2001).

Action Editor: David Golomb

Electronic supplementary material The online version of this article (doi:10.1007/s10827-016-0634-4) contains supplementary material, which is available to authorized users.

✉ Chun-Chung Chen
cjj@phys.sinica.edu.tw

¹ Institute of Physics, Academia Sinica, Nangang, Taipei, Taiwan 115, Republic of China

² Department of Physics and Center for Complex Systems, National Central University, Chungli, Taiwan 320, Republic of China

Usually, spontaneous activities can be observed after about a week *in vitro* and the activities are later synchronized into episodic network bursts (Maeda et al. 1995; Chiappalone et al. 2006). Interesting patterns of these neural bursts have been reported (Van Pelt et al. 2004; Wagenaar et al. 2006; Raichman and Ben-Jacob 2008), where the activity level of firing rate in the burst can have repeated peaks of rise-and-falls called reverberations at a time scale of hundreds of milliseconds following the initial spike of activities (Lau and Bi 2005). These so-called “super bursts” (Wagenaar et al. 2006) can last for seconds and, for their similarity in the time scales, are thought to be important to understand cognitive functions such as working memory on the cellular and network levels (Wang 2001; Lau and Bi 2005; Compte 2006; Mongillo et al. 2008; Volman and Gerkin 2011; Bermudez Contreras et al. 2013; Dranias et al. 2013).

There have been active studies on the initiation of *in vitro* neural bursts (Feinerman et al. 2007; Eckmann et al. 2008) focusing on both the role of hub neurons (Cossart 2014; Schroeter et al. 2015) and topological effects (Orlandi et al. 2013). The development of high-density MEA systems has enabled more detailed investigation of the activity propagation in the neural bursts. Notably, the collective dynamics of spiking neurons such as center-of-activity trajectory (CAT) allow the identification of a propagation phase and a reverberation phase in the progression of a burst event (Gandolfo et al. 2010).

In the current study, we use a similar high-density MEA system to investigate reverberatory bursts observed in the development of dissociated cortical cultures. Instead of considering reduced dynamics such as principal components or CAT, we use a propagation model to predict the location of each occurring spike. The effectiveness of such prediction allows the classification of the spikes into *evoked* and *spontaneous* ones, and can be used in reverse for an inference on the spreading speed of the recorded spiking activity. We find a recovering dominance of the evoked spikes over the reverberatory phase of a burst following their reduction after the initial propagating wave.

We implement a physiologically realistic model of neuronal systems (Volman et al. 2007) on a geometrically-constrained, two-dimensional network and identify sets of parameters that can produce reverberatory bursts qualitatively similar to the experimental observations. With all dynamical variables being available in computer simulations, we clarify the roles played by the neuronal noise as well as the depletion of synaptic resources in the continuation and termination of the reverberatory bursts. We find that the depletion, which is responsible for terminating the burst events (Cohen and Segal 2011), is also important in restoring the synchrony of reverberatory activity during the bursts.

2 Materials and methods

2.1 Cell cultures and experimental setup

Cortical neurons were dissociated from Wistar rat at embryonic day 17 (E17). Tissues were digested by 0.125 % trypsin and plated on the BioChip 4096E (3Brain, Switzerland) previously coated with poly-D-lysine (0.1mg/ml) and laminin (0.1 mg/ml) to promote the adhesion of neurons. About 6×10^4 neurons were plated, completely covering an active area of $6 \times 6 \text{ mm}^2$, yielding a density of the culture of about 1.7×10^3 neurons/ mm^2 . Cultures were filled with 1 mL culture medium at 30 min after plating and incubated at 37 °C in the presence of 5 % CO₂. Half of the medium was refreshed twice a week.

2.2 Electrophysiological signals

Electrophysiological activities of neurons were recorded with the original culture medium once every other day since 6 DIV in 5 % CO₂ at room temperature (24 °C). Before recording, the culture was kept at room temperature for 10 min for stabilization and placed back to the incubator immediately after the recording for future measurement. The chip 4096E has a recording area of $5.12 \times 5.12 \text{ mm}^2$ covered by 64×64 electrodes. The area of each electrode is $21 \times 21 \mu\text{m}^2$ with an inter-electrode separation of 81 μm .

The network activity was acquired at a sampling rate of 7.7 kHz for each electrode. Each recording data set includes network activity of 5 min. But, the data sets containing unstable activity patterns, long silent periods, or abnormal activities with, e.g., strong noise, were excluded for further processing. The qualified data sets for further processing are listed in Table 1. Spontaneous activities can be observed after about 2 weeks *in vitro*, comprising isolated spikes and short bursts involving many neurons (electrodes), e.g., the one shown in Fig. 1. The isolated spikes produced in neurons are detected by the BrainWave software through the Precise Timing Spike Detection with threshold values that are 8 times of the standard deviation of spike-free signals.

2.3 Detection of bursts and activity peaks

The bursts are detected as follows. The spike rate $R(t)$ at each instance t is measured as an average over the time window of size λ centered at the time. For detected spike times from each MEA recording, typically of a 5-minute duration, the maximum of the spike rate R_{max} is first determined. A lower threshold $R_{\text{lower}} \equiv \epsilon R_{\text{max}}$ is used to decide whether the culture is in an active state as illustrated in Fig. 2a. A reverberatory burst typically starts with a strong activity peak for the initiation phase followed by varying activity level or peaks in the reverberation phase as illustrated in

Table 1 List of experimental recordings

Culture	DIV	Reverberation	Spreading Speed (mm/s)
A	12	No	93.15
	25	Yes	140.9
B	13	No	30.78
	25	Yes	75.33
C	33	Yes	200.9
	40	Yes	179.8
	68	No	554.9
D	26	No	145.0
	33	Yes	458.5
	40	Yes	480.3
	68	No	517.6
E	24	Yes	77.76
	38	Yes	435.0
	41	No	398.5
F	12	Yes	116.6
	39	Yes	403.4
	54	No	448.7

Fig. 2a. A burst is registered starting at t_s when the culture becomes active at t_s and stays active until the spike rate reaches an upper threshold of $R_{upper} \equiv \Delta R_{max}$. The registered burst ends at t_e when the culture becomes inactive at t_e and stays inactive at least for a duration of τ_{term} . The empirical values for the parameters used in the burst detection of both the experimental and simulated data are: $\lambda = 0.02s$, $\epsilon = 0.04$, $\Delta = 0.2$, and $\tau_{term} = 1.5s$.

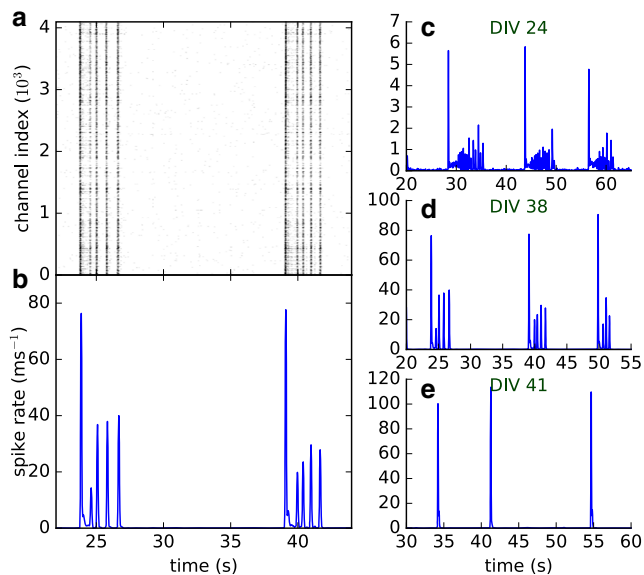


Fig. 1 **a** Raster plot of detected spikes from the culture E at DIV 38 and **b** the corresponding time histogram of firing rate. **c** to **e** Firing-rate histograms for different DIVs (as labeled) of the culture E

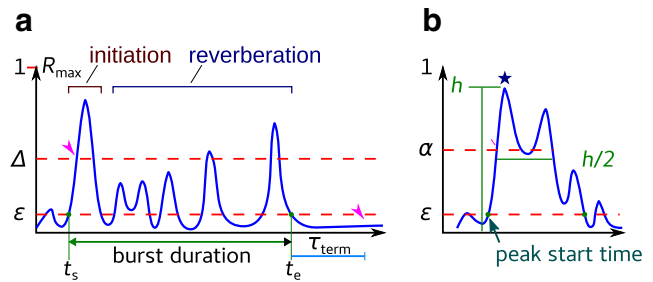


Fig. 2 Illustrated parameters for the detection of **a** a burst and **b** a spike rate peak (marked by the *star*) as described in the text. The vertical axes are spike rate in units of their maximum R_{max} of the recording while the horizontal are time axes

The peaks or reverberations could also be identified using the same method as described above with a different set of empirical parameter values. However, here we use a simpler definition that is time-symmetric: A peak is defined as a significant maximum (height $h > \alpha R_{max} > R_{lower}$) in the firing rate of a continuous time interval where the rate is above half of this maximum firing rate as marked in Fig. 2b. Preceding this interval and following the previous peak, if the firing rate of the culture stays above the lower threshold, the minimum of firing rate is considered the starting time of this peak. Otherwise, the starting time is registered as the time when the rate crosses the lower threshold. The state variables of the system representing the internal noise and degree of depletion, which are only available in simulation results, are determined at the start time of a peak to correlate with the characteristics of the peak.

2.4 Activity propagation and predictability of spiking electrodes

The propagation of the spiking activity in a burst can be visually observed from the animated replay of sustaining spikes (Supplementary Materials). To quantify the wave-like propagation of the initial sweep of activity and the subsequent distributed activation of neurons, we introduce a simple linear-spread diffusive model that can be used to predict the electrode for the next spike using spikes that have already been recorded. The probability for the next spike occurring at time t to be on the electrode at \mathbf{r} is given by

$$P(\mathbf{r}) = \frac{1}{N} \sum_{\{i|t_i < t\}} e^{-(t-t_i)/\tau_p} \frac{1}{L_i^2} e^{-|\mathbf{r}-\mathbf{r}_i|^2/L_i^2} \quad (1)$$

where t_i and \mathbf{r}_i are time and location of the previous spike i , $L_i \equiv v(t - t_i)$ is the spreading influence range of the spike i , τ_p is the decay time of the influence, $N \equiv \sum_{\mathbf{r}} P(\mathbf{r})$ is the normalization factor, and v is the spreading speed of the influence. We note that the probability (1) is conditional on a spike occurring at time t , and should be multiplied with the spike rate $R(t)$ for predicting the occurrence of a spike

at \mathbf{r} . We define the predictability of spikes as the average of $P(\mathbf{r})$ over all spikes in a recording comparing to the uniform distribution, which tells us how well the location of a spike can be predicted from previous spikes using the simple model (1). For each recording, we find the value of v that maximizes the predictability relative to a surrogate with randomized spike positions as shown in Fig. 3a and these values are included in Table 1 for all recordings. With the optimal value v , a spike is considered an evoked spike if its position \mathbf{r} satisfies $P(\mathbf{r}) > 2P_0$ where $P_0 = 1/N_{\text{elec}} \approx 2.4 \times 10^{-4}$ is the average probability for the spike to occur at an electrode out of the $N_{\text{elec}} = 4096$ electrodes for our MEA. The number ratio of evoked spikes to the total spikes within the rate peaks of a burst are shown next to the corresponding peaks in Fig. 3b.

2.5 Computer simulations

To gain insight into the dynamics of the reverberatory bursts, we use a neuronal synaptic model similar to that described by Volman et al. (2007). The model uses Morris–Lecar (ML) (Morris and Lecar 1981) neurons connected with Tsodyks–Markram (TM) (Tsodyks and Markram 1997) synapses. The dynamics of neurons are governed by the ML equations,

$$C \frac{dV}{dt} = -I_{\text{ion}} + G(V_r - V) + I_{\text{bg}}, \tag{2a}$$

$$\frac{dW}{dt} = \theta \frac{W_{\infty} - W}{\tau_W} \tag{2b}$$

where

$$I_{\text{ion}} = g_{\text{Ca}} m_{\infty} (V - V_{\text{Ca}}) + g_{\text{K}} W (V - V_{\text{K}}) + g_{\text{L}} (V - V_{\text{L}}) \tag{3}$$

is the current through the membrane ion channels,

$$\tau_W = \left(\cosh \frac{V - V_3}{2V_4} \right)^{-1}, \tag{4a}$$

$$W_{\infty} = \frac{1}{2} \left(1 + \tanh \frac{V - V_3}{V_4} \right), \tag{4b}$$

$$m_{\infty} = \frac{1}{2} \left(1 + \tanh \frac{V - V_1}{V_2} \right) \tag{4c}$$

are the voltage dependent dynamic parameters, and the threshold V_{th} of membrane potential defines the spiking events which result in synchronous releases of neural transmitters at the efferent synapses. Additionally, a residual calcium variable R_{Ca} driven by the spiking events,

$$\frac{d}{dt} R_{\text{Ca}} = \frac{-\beta R_{\text{Ca}}^n}{k_R^n + R_{\text{Ca}}^n} + I_p + S\gamma \log \frac{R_{\text{Ca}}^0}{R_{\text{Ca}}}, \tag{5}$$

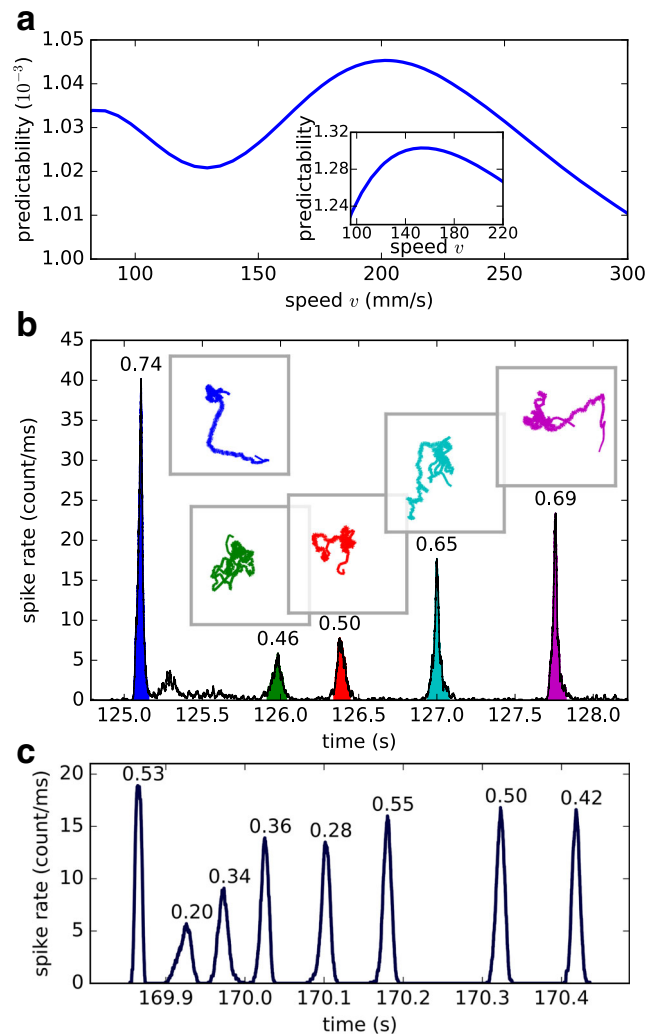


Fig. 3 **a** Predictability as a function of presumed spreading speed for culture C at 33 DIV. *Inset* is a similar plot from a simulation. **b** Time-histogram of a typical reverberatory burst with identified activity peaks color coded with corresponding center-of-activity trajectories in the insets. The numbers next to the rate peaks show the fractions of the evoked spikes out of all spikes in the activity peaks. **c** Time-histogram for a simulated reverberatory burst. The fractions of evoked spikes are similarly labeled for each activity peak

where the spike train is $S = \sum_{\sigma} \delta(t - t_{\sigma})$ with t_{σ} being the time of the spike event σ , is used to determine the rate,

$$\eta = \eta_{\text{max}} \frac{R_{\text{Ca}}^m}{k_a^m + R_{\text{Ca}}^m}, \tag{6}$$

of synapse-dependent asynchronous releases of neural transmitters (see below) following an independent Poisson process at each efferent synapse. The neural transmitters released by the spike-driven synchronous and calcium-

dependent asynchronous events follow a four-state decaying dynamics based on a modification of the TM model,

$$\frac{dX}{dt} = \frac{Q}{\tau_s} + \frac{Z}{\tau_r} - uXS - X\xi \tag{7a}$$

$$\frac{dY}{dt} = -\frac{Y}{\tau_d} + uXS + X\xi \tag{7b}$$

$$\frac{dZ}{dt} = \frac{Y}{\tau_d} - \frac{Z}{\tau_r} - \frac{Z}{\tau_l} \tag{7c}$$

$$\frac{dQ}{dt} = \frac{Z}{\tau_l} - \frac{Q}{\tau_s} \tag{7d}$$

where $\xi = \bar{\xi} \sum_a \delta(t - t_a)$ summing over the asynchronous release events a with a Poisson rate given by (6), to include a super-inactive state Q . Multiplying by the synaptic weights, the fractions of neural transmitters in the active state Y (7b) determine the contribution of the afferent synapses to the membrane conductance G of a post-synaptic neuron through a linear sum

$$G_i = \sum_j w_{ji} Y_{ji} \tag{8}$$

over all pre-synaptic neurons j of the given post-synaptic neuron i . Following Volman et al. (2007), the synaptic weights w are randomly drawn from a truncated Gaussian distribution with a width that is $\pm 20\%$ of its mean \bar{w} for the connected neurons.

We place the model neurons on a 2D geometrical network with connection probability between two neurons decaying exponentially with the distance between them. Most of the model parameters used in our simulations follow the values given in (Volman et al. 2007) and can be found in Table 2. The time constants of TM dynamics, background currents for ML neurons, and synaptic weights are adjusted uniformly to reach simulated time-histograms that qualitatively reproduce the experimental results as seen in Fig. 3.

Table 2 Values of parameters used in simulations

Morris–Lecar model					
V_{Ca}	100 mV	V_2	15 mV	g_L	0.5 mS
V_K	-70 mV	V_3	0 mV	C	1 μ F
V_L	-65 mV	V_4	30 mV	θ	0.2 ms^{-1}
V_r	0 mV	g_{Ca}	1.1 mS	V_{th}	10 mV
V_l	-1 mV	g_K	2 mS		
Tsodyks–Markram synaptic transmission					
τ_d	10 ms	τ_l	800 ms	u	0.25
τ_r	250 ms	τ_s	5000 ms	$\bar{\xi}$	0.02
Residual calcium dynamics					
β	0.005 $\frac{\mu M}{ms}$	γ	0.033	k_a	0.13 μM
k_R	0.4 μM	R_{Ca}^0	2000 μM	m	4
I_p	1.1×10^{-4} $\frac{\mu M}{ms}$	η_{max}	0.32 ms^{-1}	n	2

The raster plots for the simulated burst and the experimentally observed burst in Fig. 3 are shown in Fig. 4. For current study, we focus on the reverberatory bursts with distinct reverberation peaks or sub-bursts in the spike rate histogram.

The same burst and peak detections for the experimental measurements are applied to the simulation results with slightly different empirical parameters. Comparing to the experiments, the full dynamics of the simulations is readily available as numerical data and can be further analyzed to clarify the physical mechanisms of the bursting behavior. Beside recording the time and neuron of each spike for the calculation of a time-histogram and keeping track of activity propagation, we are interested in the information of neuronal noise and the depletion of synaptic resources. The former is represented by the average concentration of residual calcium that governs the asynchronous release while the later is represented by the average fraction of inactive and super inactive neural transmitters which deplete the available neural transmitters in a bursting cycle. Both of the values are retained at the start time of each detected peak in the spike-rate histogram and used to correlate with the properties of each peak.

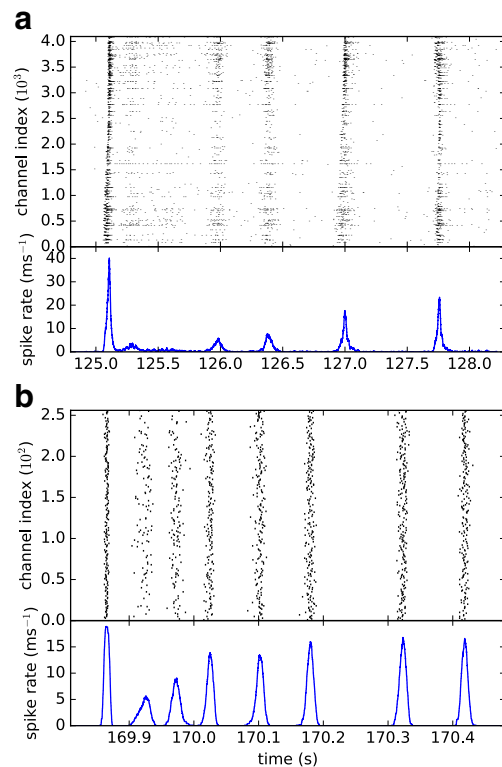


Fig. 4 **a** Raster plot of recorded spikes and corresponding spike-rate histogram for the bursting event shown in Fig. 3b. **b** Raster plot of simulated spikes and corresponding histogram for the bursting event shown in Fig. 3c

2.6 Implementations

We implemented the computational model in the C++ programming language using the Common Simulation Tools framework (Chen 2016a). The simulation codes and the framework are available on the github (Chen 2016b). A brief description of the structure of the code, the data file of the simulated system, and animated propagations for a simulated and an experimental burst are included in the [Supplementary Materials](#) of the paper. The spike data from the MEA recordings as well as the computer simulations were processed with the Python3 programming language and most of the data plots were produced using the Matplotlib library module. A Jupyter Notebook containing the Python3 codes for data processing and plotting is also included in the [Supplementary Materials](#).

3 Results

After plating, spontaneous activities are observed in about a week *in vitro*. Such activities become synchronized into network bursts around 10 DIV and show reverberations after 15 DIV. The number of peaks per burst reaches a maximum around 30 DIV as shown in Fig. 5 and falls back to one without reverberation after 40 DIV. It has been observed that the reverberatory bursts during the intermediate DIV can be divided into two phases (Gandolfo et al. 2010): a propagation phase where the channels are activated sequentially and diffusively and a reverberation phase where the firings of the neurons are seemingly random and more decoupled. Such division was confirmed with CAT observation. As evident from stretches of the CATs shown in the insets of Fig. 3b for a reverberatory burst, the propagation is indeed more prominent for the initiating peak of spike rate (blue trajectory) and

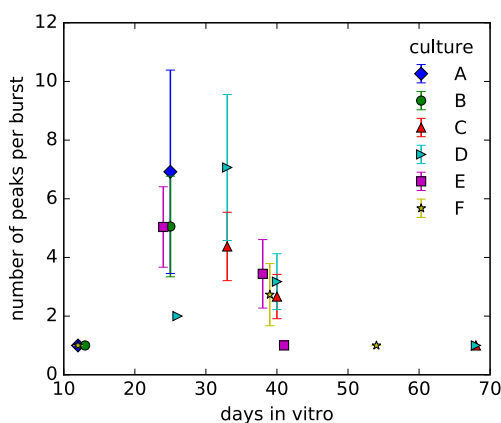


Fig. 5 Number of detected peaks in spike rate per burst as a function of DIV of the cultures. The reverberation of the bursts is maximized around 30 DIV

reduces to a lingering (green) trajectory soon after. However, as the network reverberates, the CAT gradually regains its propagating sweeps until the end of the burst (magenta trajectory).

The factors driving the spiking activity of a neuron during a bursting event include the synaptic action spreading from its presynaptic neurons and the spontaneous activation driven by its own neuronal or synaptic noises. To identify the dominating factor contributing to a spike, we use the simple linear-spread diffusive model (1) parametrized with a spreading speed, which can be determined by a maximum likelihood method for each recording as documented in Table 1. While a more sophisticated propagation model might produce a better match to the observed behavior, the added complexity is not expected to change our conclusions qualitatively. Using the propagation model (1), we classify spikes into evoked spikes and spontaneous spikes. We then determine their ratio for all rate peaks of a burst. The results of evoked-spike fractions plotted in Fig. 6a for 33 DIV recording of culture C show an increase in the fraction of evoked spikes as the network reverberates. To characterize how synchronous the spikes within an activity peak are, we normalize each rate peak i with its spike count n_i and use the normalized height h_i/n_i to quantify the synchrony. In Fig. 6b, the synchrony of the activity peaks is plotted against the time of the peaks relative to the start of the bursts. While the synchrony data is more disperse, we can see an upward trend following the time course of the bursts. This demonstrates a correlation between the activ-

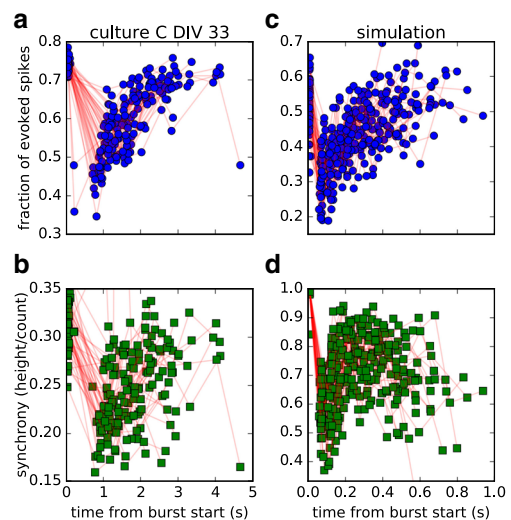


Fig. 6 **a** Fraction of evoked spikes in detected activity peaks for reverberatory bursts of 33 DIV recording of culture C against the peak times relative to the start of the bursts. **b** Peak synchrony defined as the height of a peak over its spike count. The faint lines connect activity peaks in a burst in sequence. **c** and **d** are corresponding results for fraction of evoked spikes and synchrony, respectively, from simulations

ity spreading and synchrony of the spikes. The result may not be a surprise considering the activity spreading through synaptic action following presynaptic spikes is how neurons can communicate and should help to orchestrate the synchronous activity.

To further clarify the synaptic dynamics contributing to the increasing dominance of the evoked spikes over spontaneous ones during a reverberatory burst, we turn to our simulations that produce qualitatively similar, reverberatory bursts with the increasing height of activity peaks in the spike-rate, time histogram over the bursts as shown in Fig. 3c. With a simulated system, the full set of dynamic variables are available for analysis. We identify two factors of relevance in determining the peak height or the synchrony of the reverberation from our simulations: Firstly, the residual calcium concentration controls the rate of asynchronous release at synapses in the model and represents the strength of an internal *noise* of the neurons. Secondly, the inactive and super-inactive states featured in the model take up the neural transmitters as they are activated and represent the *depletion* of synaptic resources. We correlate the system average of these two factors with the height of activity peaks in a 3D scatter plot for all peaks of the

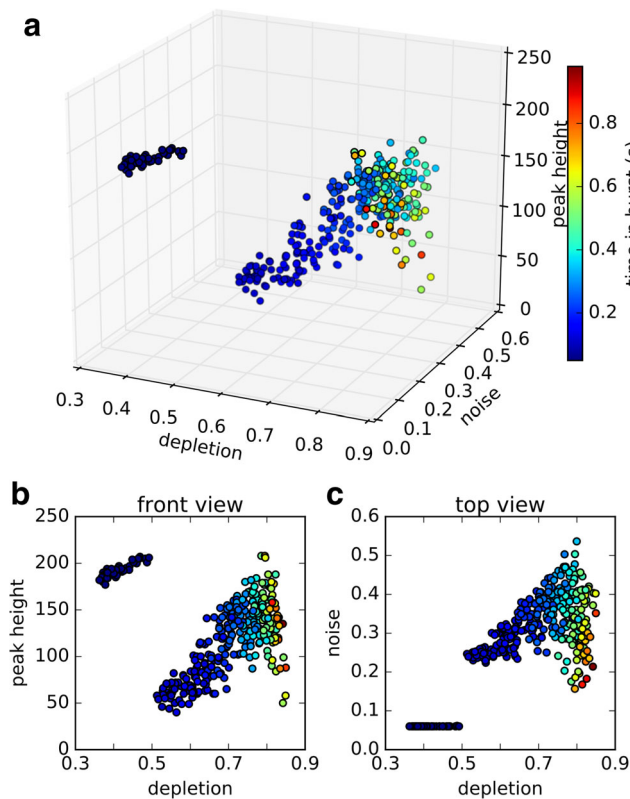


Fig. 7 **a** Scatter plot for correlation of height of activity peaks with the system level of noise, represented by residual calcium concentration ($[Ca^{2+}]$), and the depletion of synaptic resources, represented by the super inactive state of neural transmitters. **b** Front view of the 3D plot. **c** Top view of the 3D plot

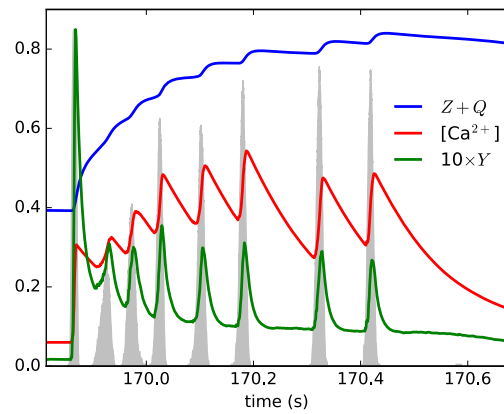


Fig. 8 Average levels of residual calcium concentration (*middle curve*), depleted neural transmitter (*upper curve*), and active neural transmitter fractions (*lower curve*, 10-time magnified) of the system over the course of the simulated burst of Fig. 3c. The *shaded area* shows the time-histogram of the burst

simulated recording as shown in Fig. 7. From the projection Fig. 7b, we see that depletion, which increases during a burst, correlates positively with an increase of the peak height and thus the synchrony of the spikes. On the other hand, the noise factor represented by residual calcium, as shown in Fig. 7c, is initially pumped up by the spiking activity of a burst, reaching a maximum about half way through the burst, and decreases afterward due to the lengthening intervals between the reverberation peaks until the end of the burst.

The detailed dynamics of different factors can be further analyzed in a simulation. In Fig. 8, we plot the residual calcium concentration, depleted neural transmitter fraction ($Z + Q$), and the active neural transmitter fraction over the very burst shown in Fig. 3c. Taken from the computational model, the depletion of neural transmitters to the Z and Q states is driven by the activated transmitters Y from the spiking activity. The spiking activity also increases the level of residual calcium, which controls the noisy, asynchronous releases of the neural transmitters leading to the reverberation in a burst. Apart from making the role of synchronous releases more important in the activation of neurons, the depletion also leads to longer recovery time of neural transmitters. Coupling with the rapid decay of calcium between the reverberation peaks, this leads to the lowering in the mean level of residual calcium towards the end of a burst.

4 Discussion

In the current study, we use a high-density MEA system to investigate the physical mechanisms underlying the morphological richness of reverberatory neural bursts. Our simple linear-spread diffusive model allows a classification of the spikes as well as an inference of the propagation speed of

synaptic activities. The change of the predictability of spikes allows us to detect the change in the propagation behavior during a burst as shown in Fig. 6. However, the traveling-wave-like sweep of activity, especially for the initiation of a burst, is not diffusive. A more sophisticated model will be required if one would like to have a more faithful capture of such dynamics. Nonetheless, the method of inference for the model parameters using individual spikes as demonstrated remains applicable. The method is enabled by our use of high-density MEA and does not resort to data reduction before inferring the propagation dynamics. That is, each spike has a direct contribution to the resolution of the spreading speed and the method can potentially be used to resolve more complex dynamics of the system.

The finding from our analysis of the simulated system suggests an interesting phenomena, which we call *depletion-enhanced synchronization*, at play in the cultured network with the reverberatory bursts. In such a burst, the initiation activity is a fast sweeping wave of propagating spikes across the network that is well synchronized. This activity produces a significant amount of residual calcium, promoting noisy asynchronous releases, and prompting the spontaneous firing of the neurons that results in the subsequent reverberation of the burst. Initially, the spontaneous spikes are more or less independent and the heterogeneity in the neurons and their connectivity makes the spike-rate peaks broad and less synchronous. However, as the neural and synaptic resources are increasingly depleted by the continuing spiking activity of the burst, it becomes harder for the neurons to fire independently and they thus increasingly rely on the synchronous releases triggered by the firing of their presynaptic neurons to help them cross the firing threshold. Such mechanism accounts for the observed increase of evoked spikes and the synchrony in Fig. 6 and may be a general mode of operation for other complex systems.

The synchronized network activities observed in our cultures seem to be similar to the switching between Up and Down states as observed in other neuronal network preparations (MacLean et al. 2005; Holcman and Tsodyks 2006; Johnson and Buonomano 2007). However, since our measurements are carried out on MEA, records of the membrane potentials are not available to verify these states. It is known that activities similar to what we reported here can also be induced in acute slice (Czarnecki et al. 2012) when inhibitory interactions are blocked. Presumably, there are too many recurrent connections in our cultures which might correspond to the pathological condition during epilepsy (McCormick and Contreras 2001).

In the computational model, the active state is initially stabilized by the residual calcium which promotes the asynchronous releases intrinsic to the neurons, and later revitalized by the synaptic couplings of the network. The role of

calcium in the reverberation was implicated by Lau and Bi (2005) and we chose to implement the model by Volman et al. (2007) based the similarity between the firing-rate time histograms it produces and those were seen in our experiments. Alternatively, NMDA receptors have been proposed to play a role in persisting a burst (Wang 1999, 2001). It will be interesting to see in future studies what difference in the bursting morphology will result from an NMDA receptor based model.

Finally, we note that while synchrony is often associated with coherence, it actually reduces the diversity in the possible dynamics of a system. In the reverberatory bursts that we focused on, the synchrony results from the depletion of synaptic resources and precedes the termination of the burst. This parallels the recent findings in epilepsy that increasing synchrony can be observed towards the end of seizures (Lehnertz et al. 2009; Jiruska et al. 2013). Our results may suggest a possible mechanism for such phenomena for systems of similar episodic dynamics.

Acknowledgments This work has been supported by the Ministry of Science and Technology, Taiwan, Republic of China under grand no. 102-2112-M-001 -009 -MY3, and Physics Division, National Center for Theoretical Sciences, Taiwan, Republic of China.

Compliance with Ethical Standards

Conflict of interests The authors declare that they have no conflict of interest.

References

- Bermudez Contreras, E.J., Schjetnan, A.G.P., Muhammad, A., Bartho, P., McNaughton, B.L., Kolb, B., Gruber, A.J., & Luczak, A. (2013). Formation and reverberation of sequential neural activity patterns evoked by sensory stimulation are enhanced during cortical desynchronization. *Neuron*, 79(3), 555–566.
- Bi, G.Q., & Poo, M.M. (2001). Synaptic modification by correlated activity: Hebb's postulate revisited. *Annual Review of Neuroscience*, 24(1), 139–166.
- Blankenship, A.G., & Feller, M.B. (2010). Mechanisms underlying spontaneous patterned activity in developing neural circuits. *Nature Reviews Neuroscience*, 11(1), 18–29.
- Chen, C.C. (2016a). chnchg/cst: common simulation tools. *Zenodo*. doi:10.5281/zenodo.163650.
- Chen, C.C. (2016b). chnchg/measim: simulation of two-dimensional cultured neuronal network. *Zenodo*. doi:10.5281/zenodo.166691.
- Chiappalone, M., Bove, M., Vato, A., Tedesco, M., & Martinoia, S. (2006). Dissociated cortical networks show spontaneously correlated activity patterns during *in vitro* development. *Brain Research*, 1093(1), 41–53.
- Cohen, D., & Segal, M. (2011). Network bursts in hippocampal microcultures are terminated by exhaustion of vesicle pools. *Journal of Neurophysiology*, 106(5), 2314–2321.
- Compte, A. (2006). Computational and *in vitro* studies of persistent activity: edging towards cellular and synaptic mechanisms of working memory. *Neuroscience*, 139(1), 135–151.

- Cossart, R. (2014). Operational hub cells: a morpho-physiologically diverse class of GABAergic neurons united by a common function. *Current Opinion in Neurobiology*, 26, 51–56.
- Crair, M.C. (1999). Neuronal activity during development: permissive or instructive? *Current Opinion in Neurobiology*, 9(1), 88–93.
- Czarnecki, A., Tscherter, A., & Streit, J. (2012). Network activity and spike discharge oscillations in cortical slice cultures from neonatal rat. *European Journal of Neuroscience*, 35(3), 375–388.
- Dranias, M.R., Ju, H., Rajaram, E., & VanDongen, A.M.J. (2013). Short-Term memory in networks of dissociated cortical neurons. *The Journal of Neuroscience*, 33(5), 1940–1953.
- Eckmann, J.P., Jacobi, S., Marom, S., Moses, E., & Zbinden, C. (2008). Leader neurons in population bursts of 2d living neural networks. *New Journal of Physics*, 10(1), 015,011.
- Feinerman, O., Segal, M., & Moses, E. (2007). Identification and dynamics of spontaneous burst initiation zones in unidimensional neuronal cultures. *Journal of Neurophysiology*, 97(4), 2937–2948.
- Gandolfo, M., Maccione, A., Tedesco, M., Martinoia, S., & Berdoncini, L. (2010). Tracking burst patterns in hippocampal cultures with high-density CMOS-MEAs. *Journal of Neural Engineering*, 7(5), 056,001.
- Gross, G.W., Williams, A.N., & Lucas, J.H. (1982). Recording of spontaneous activity with photoetched microelectrode surfaces from mouse spinal neurons in culture. *Journal of Neuroscience Methods*, 5(1), 13–22.
- Harris, W.A. (1981). Neural activity and development. *Annual Review of Physiology*, 43(1), 689–710.
- Holcman, D., & Tsodyks, M. (2006). The emergence of up and down states in cortical networks. *PLoS Comput Biol*, 2(3), e23.
- Hua, J.Y., & Smith, S.J. (2004). Neural activity and the dynamics of central nervous system development. *Nature Neuroscience*, 7(4), 327–332.
- Jiruska, P., de Curtis, M., Jefferys, J.G.R., Schevon, C.A., Schiff, S.J., & Schindler, K. (2013). Synchronization and desynchronization in epilepsy: controversies and hypotheses. *The Journal of Physiology*, 591(4), 787–797.
- Johnson, H.A., & Buonomano, D.V. (2007). Development and plasticity of spontaneous activity and up states in cortical organotypic slices. *The Journal of Neuroscience*, 27(22), 5915–5925.
- Katz, L.C., & Shatz, C.J. (1996). Synaptic activity and the construction of cortical circuits. *Science*, 274(5290), 1133–1138.
- Kerschensteiner, D. (2014). Spontaneous network activity and synaptic development. *The Neuroscientist*, 20(3), 272–290.
- Lau, P.M., & Bi, G.Q. (2005). Synaptic mechanisms of persistent reverberatory activity in neuronal networks. *Proceedings of the National Academy of Sciences*, 102(29), 10,333–10,338.
- Lehnertz, K., Bialonski, S., Horstmann, M.T., Krug, D., Rothkegel, A., Staniek, M., & Wagner, T. (2009). Synchronization phenomena in human epileptic brain networks. *Journal of Neuroscience Methods*, 183(1), 42–48.
- MacLean, J.N., Watson, B.O., Aaron, G.B., & Yuste, R. (2005). Internal dynamics determine the cortical response to thalamic stimulation. *Neuron*, 48(5), 811–823.
- Maeda, E., Robinson, H.P.C., & Kawana, A. (1995). The mechanisms of generation and propagation of synchronized bursting in developing networks of cortical neurons. *Journal of Neuroscience*, 15(10), 6834–6845.
- McCormick, D.A., & Contreras, D. (2001). On the cellular and network bases of epileptic seizures. *Annual Review of Physiology*, 63(1), 815–846.
- Meister, M., Wong, R.O., Baylor, D.A., & Shatz, C.J. (1991). Synchronous bursts of action potentials in ganglion cells of the developing mammalian retina. *Science*, 252(5008), 939–943.
- Mongillo, G., Barak, O., & Tsodyks, M. (2008). Synaptic theory of working memory. *Science*, 319(5869), 1543–1546.
- Morris, C., & Lecar, H. (1981). Voltage oscillations in the barnacle giant muscle fiber. *Biophysical Journal*, 35(1), 193–213.
- Orlandi, J.G., Soriano, J., Alvarez-Lacalle, E., Teller, S., & Casademunt, J. (2013). Noise focusing and the emergence of coherent activity in neuronal cultures. *Nature Physics*, 9(9), 582–590.
- Penn, A.A., & Shatz, C.J. (1999). Brain waves and brain wiring: the role of endogenous and sensory-driven neural activity in development. *Pediatric Research*, 45(4, Part 1 of 2), 447–458.
- Pine, J. (1980). Recording action potentials from cultured neurons with extracellular microcircuit electrodes. *Journal of Neuroscience Methods*, 2(1), 19–31.
- Potter, S.M., & DeMarse, T.B. (2001). A new approach to neural cell culture for long-term studies. *Journal of Neuroscience Methods*, 110(1–2), 17–24.
- Pu, J., Gong, H., Li, X., & Luo, Q. (2013). Developing neuronal networks: self-organized criticality predicts the future. *Scientific Reports*, 3.
- Raichman, N., & Ben-Jacob, E. (2008). Identifying repeating motifs in the activation of synchronized bursts in cultured neuronal networks. *Journal of Neuroscience Methods*, 170(1), 96–110.
- Schroeter, M.S., Charlesworth, P., Kitzbichler, M.G., Paulsen, O., & Bullmore, E.T. (2015). Emergence of rich-club topology and coordinated dynamics in development of hippocampal functional networks *in vitro*. *The Journal of Neuroscience*, 35(14), 5459–5470.
- Segev, R., Benveniste, M., Shapira, Y., & Ben-Jacob, E. (2003). Formation of electrically active clustered neural networks. *Physical Review Letters*, 90(16), 168,101.
- Thomas, C.A., Springer, P.A., Loeb, G.E., Berwald-Netter, Y., & Okun, L.M. (1972). A miniature microelectrode array to monitor the bioelectric activity of cultured cells. *Experimental Cell Research*, 74(1), 61–66.
- Tsodyks, M.V., & Markram, H. (1997). The neural code between neocortical pyramidal neurons depends on neurotransmitter release probability. *Proceedings of the National Academy of Sciences*, 94(2), 719–723.
- Turrigiano, G.G., & Nelson, S.B. (2004). Homeostatic plasticity in the developing nervous system. *Nature Reviews Neuroscience*, 5(2), 97–107.
- Van Pelt, J., Corner, M.A., Wolters, P.S., Rutten, W.L.C., & Ramakers, G.J.A. (2004). Longterm stability and developmental changes in spontaneous network burst firing patterns in dissociated rat cerebral cortex cell cultures on multielectrode arrays. *Neuroscience Letters*, 361(1–3), 86–89.
- Volman, V., & Gerkin, R.C. (2011). Synaptic scaling stabilizes persistent activity driven by asynchronous neurotransmitter release. *Neural Computation*, 23(4), 927–957.
- Volman, V., Gerkin, R.C., Lau, P.M., Ben-Jacob, E., & Bi, G.Q. (2007). Calcium and synaptic dynamics underlying reverberatory activity in neuronal networks. *Physical Biology*, 4(2), 91–103.
- Wagenaar, D.A., Pine, J., & Potter, S.M. (2006). An extremely rich repertoire of bursting patterns during the development of cortical cultures. *BMC Neuroscience*, 7(1), 11.
- Wang, X.J. (1999). Synaptic basis of cortical persistent activity: the importance of NMDA receptors to working memory. *The Journal of Neuroscience*, 19(21), 9587–9603.
- Wang, X.J. (2001). Synaptic reverberation underlying mnemonic persistent activity. *Trends in Neurosciences*, 24(8), 455–463.
- Zhang, L.I., & Poo, M.M. (2001). Electrical activity and development of neural circuits. *Nature Neuroscience*, 4, 1207–1214.